



# Untargeted metabolomics unveil alterations of biomembranes permeability in human HaCaT keratinocytes upon 60 GHz millimeter-wave exposure

Pierre Le Pogam, Yann Le Page, Denis Habauzit, Mickael Doué, Maxim Zhadobov, Ronan Sauleau, Yves Le Dréan, David Rondeau

## ► To cite this version:

Pierre Le Pogam, Yann Le Page, Denis Habauzit, Mickael Doué, Maxim Zhadobov, et al.. Untargeted metabolomics unveil alterations of biomembranes permeability in human HaCaT keratinocytes upon 60 GHz millimeter-wave exposure. *Scientific Reports*, 2019, 9 (1), pp.9343. 10.1038/s41598-019-45662-6 . hal-02179383

HAL Id: hal-02179383

<https://univ-rennes.hal.science/hal-02179383>

Submitted on 7 Jul 2020

**HAL** is a multi-disciplinary open access archive for the deposit and dissemination of scientific research documents, whether they are published or not. The documents may come from teaching and research institutions in France or abroad, or from public or private research centers.

L'archive ouverte pluridisciplinaire **HAL**, est destinée au dépôt et à la diffusion de documents scientifiques de niveau recherche, publiés ou non, émanant des établissements d'enseignement et de recherche français ou étrangers, des laboratoires publics ou privés.

# SCIENTIFIC REPORTS



OPEN

## Untargeted metabolomics unveil alterations of biomembranes permeability in human HaCaT keratinocytes upon 60 GHz millimeter-wave exposure

Pierre Le Pogam<sup>1</sup>, Yann Le Page<sup>2</sup>, Denis Habauzit<sup>2</sup>, Mickael Doué<sup>1</sup>, Maxim Zhadobov<sup>1</sup>, Ronan Sauleau<sup>1</sup>, Yves Le Dréan<sup>2</sup> & David Rondeau<sup>1,3</sup>

A joint metabolomic and lipidomic workflow is used to account for a potential effect of millimeter waves (MMW) around 60 GHz on biological tissues. For this purpose, HaCaT human keratinocytes were exposed at 60.4 GHz with an incident power density of 20 mW/cm<sup>2</sup>, this value corresponding to the upper local exposure limit for general public in the context of a wide scale deployment of MMW technologies and devices. After a 24h-exposure, endo- and extracellular extracts were recovered to be submitted to an integrative UPLC-Q-Exactive metabolomic and lipidomic workflow. R-XCMS data processing and subsequent statistical treatment led to emphasize a limited number of altered features in lipidomic sequences and in intracellular metabolomic analyses, whatever the ionization mode (*i.e.* 0 to 6 dysregulated features). Conversely, important dysregulations could be reported in extracellular metabolomic profiles with 111 and 99 frames being altered upon MMW exposure in positive and negative polarities, respectively. This unexpected extent of modifications can hardly stem from the mild changes that could be reported throughout transcriptomics studies, leading us to hypothesize that MMW might alter the permeability of cell membranes, as reported elsewhere.

Owing to the saturation of the lower part of the microwave spectrum and to the growing demand for higher data rates, the millimeter waves (MMW) are increasingly used for wireless communications, *i.e.* for Wireless Local/Personal/Body Area Networks (WLAN, PAN, BAN) or in the context of the upcoming 5 G mobile standard<sup>1</sup>. These electromagnetic radiations correspond to frequencies ranging from 30 to 300 GHz (free-space wavelengths spanning from 10 to 1 mm). Interestingly, MMW have been used for therapeutic purposes indicating that physiological processes might be altered upon exposure to these radiations<sup>2</sup>. Accordingly, the assessment of the potential effects of MMW on human health is thus of paramount importance prior to the wide scale deployment of technologies exploiting this band. MMW are known for their shallow penetration of human tissues (between a few tenth of millimeter to a millimeter), making skin keratinocytes and free nerve endings the primary targets for MMW<sup>3</sup>. It is assumed that some general effects of MMW may be initiated by the release of skin-secreted factors into the blood stream or through the stimulation of superficial free nerve endings<sup>4,5</sup>.

The shallow penetration depth of MMW in skin, results in elevated levels of Specific Absorption Rates (SAR) compared to lower microwave frequencies with the same Incident Power Density (IPD). As a consequence, this leads to a noticeable local heating for IPD exceeding typically 5 mW/cm<sup>2</sup><sup>6</sup>. Accordingly, one of the main safety concerns regarding these frequencies is the local heating of skin caused by the absorption of MMW energy in the human body<sup>7</sup>. Whether electromagnetic-field specific effects occur upon exposure to MMW<sup>8–12</sup> or not<sup>13–17</sup> has been a matter of debate for a long period of time. Besides the warm-up effect, the mechanisms accounting for

<sup>1</sup>Univ Rennes, CNRS, IETR (Institut d'Électronique et de Télécommunication de Rennes), UMR 6164, F-35000, Rennes, France. <sup>2</sup>Univ Rennes, Inserm, EHESP, Iset (Institut de recherche en santé, environnement et travail) – UMR\_S 1085, F-35000, Rennes, France. <sup>3</sup>Département de Chimie, Université de Bretagne Occidentale, 6 avenue Victor Le Gorgeu, 29238, Brest, Cedex, France. Correspondence and requests for materials should be addressed to D.R. (email: [david.rondeau@univ-rennes1.fr](mailto:david.rondeau@univ-rennes1.fr))

Metabolome	Fraction	Ion mode	Ions	Ions with CV QC < 30% (% of total ions)	Ions with both CV QC < 30% and FC > 2
Exo	Lipido	Positive	3081	2161 (70.82)	289
		Negative	1920	1126 (56.25)	126
	Metabo	Positive	2750	2076 (75.42)	662
		Negative	1632	1263 (77.37)	506
Endo	Lipido	Positive	4295	3920 (91.27)	540
		Negative	2468	2164 (87.68)	264
	Metabo	Positive	1910	1525 (79.84)	210
		Negative	1017	843 (83.00)	58

**Table 1.** Validation of the generated data set using R-XCMS data processing.

non-thermal effects occurring at low-power exposure have not been fully demonstrated yet so that their understanding remains an open challenge<sup>18</sup>. Consequently, the guidelines established by the International Commission on Non Ionizing Radiation Protection (ICNIRP) aim at circumventing thermal hazards associated with MMW exposure. This led to define two exposure scenarios. For far-field exposure, the IPD is limited to 1 mW/cm<sup>2</sup>. For body-centric wireless networks that are related to very limited exposition area, the IPD limit is set at 20 mW/cm<sup>2</sup> (averaged over 1 cm<sup>2</sup>). While such exposure scenarios may trigger a heat-shock response, it is assumed that the thermoregulation due to blood flow effect might be efficient to avoid any thermal damage.

Notwithstanding decades of investigations and a significant number of studies dedicated at unravelling the effects of MMW on biosystems, the number of reliable and reproducible experimental data remains scarce, most likely stemming from difficulties in dissociating thermal and electromagnetically pure effects. Our group aimed at evaluating the biological effects of MMW in the 60 GHz band. Previous *in vitro* studies revealed that MMW at 57–64 GHz exert no influence on protein homeostasis for IPD low enough to prevent any temperature increase<sup>19–21</sup>. Moreover, transcriptomic studies highlighted no, or very weak, effect of MMW on keratinocyte gene expression under athermal conditions<sup>22–24</sup>. By contrast, it must be mentioned that some authors have pointed out the MMW effects on cell membranes, indicating that permeability changes could be induced by a direct effect on membrane proteins or phospholipids domain organization<sup>25</sup>. The possibility of permeation across the lipid bilayer led us to consider the metabolomic profiling of human keratinocytes as a pertinent next step to better understand the interactions between MMW radiation and cell membrane in the context of human body exposure to 60 GHz waves. The goal of the present study is to apply an untargeted metabolomic strategy based on UHPLC-HRMS assessment of metabolic changes appearing upon exposure to MMW in human HaCaT keratinocytes cell lines. Cells were exposed at 60.4 GHz with an IPD of 20 mW/cm<sup>2</sup> with the temperature being artificially maintained constant between non-exposed and exposed samples<sup>26</sup>. As metabolites represent the sharp end of systems biology, including multiple up-stream steps, the keratinocytes were exposed for 24 hours to enable possible changes. Then, to afford as wide a coverage of HaCaT keratinocytes chemistry as possible, lipidomic and metabolomic profilings were performed in both intra- and extracellular fractions in positive and negative polarities using a metabolomic workflow that we had previously validated<sup>27</sup>.

## Results and Discussion

**Data quality assurance.** The analytical strategy adopted herein was based on two different chromatographic separation methods (HILIC and RPLC, see experimental section) coupled to detection in mass spectrometry involving both positive and negative-ion modes. This strategy was applied by distinguishing the endo- and exocellular fractions as well to deepen the coverage of the metabolome. As a result, this led to analyze each biological sample 8 times, in distinct sessions of analyses.

Prior to any data processing or analysis, several quality checks were adopted (*i.e* column pressure checking, variations of internal standards in QC/study samples and instrumental stability in terms of retention time and accurate masses) along the whole batch. Accordingly, internal standards were spiked into each sample prior to LC-HRMS analyses to assess retention time stability, the consistency of signal intensities and mass accuracy along the whole batch. No significant drift in retention time could be evidenced. Likewise, standard accurate mass measurements errors always remained below 5 ppm. For metabolomic analyses, the selected external standards were leucine-d<sub>3</sub> (RT 5.97 min), tryptophan-d<sub>3</sub> (RT 6.10 min), indole acetic acid-d<sub>5</sub> (RT, 1.81 min) and tetradecanedioic acid-d<sub>24</sub> (RT 1.38 min). Creatine-d<sub>3</sub> (RT 8.22 min) and L-lysine-d<sub>4</sub> (RT 14.31 min) were selected as internal standards. As to lipidomic sequences, phosphatidylcholine (15:0) (RT 8.37 min), lysophosphatidylcholine (15:0) (RT 1.75 min), ceramide (d18:1) (RT 17.95 min), C15:0 (RT 3.19 min) and C23:0 (RT 9.27 min) were used as external standards, whereas C17:0 (RT 4.30 min) served as an internal standard. All these standards revealed a coefficient of variation below 30% except in the case of C17:0 which displayed a slightly higher value in negative-ion mode of the exo-lipidomics sequence (33.7%) (Tables S1 and S2).

The analysis of QC samples served as a further criterion to establish both the quality of the generated data and the stability of the instrumental platform. For this purpose, it is highly recommended that QC peak tables should pass pre-determined criteria, a widely admitted one being that a majority of features (*i.e.* 70%) shows a coefficient of variation less than 30%<sup>28</sup>. With respect to this parameter, most sequences displayed satisfying values, with only negative-ion mode exo-lipidomics sequence exhibiting a slightly lower value of 56.3% (Table 1). The stability of

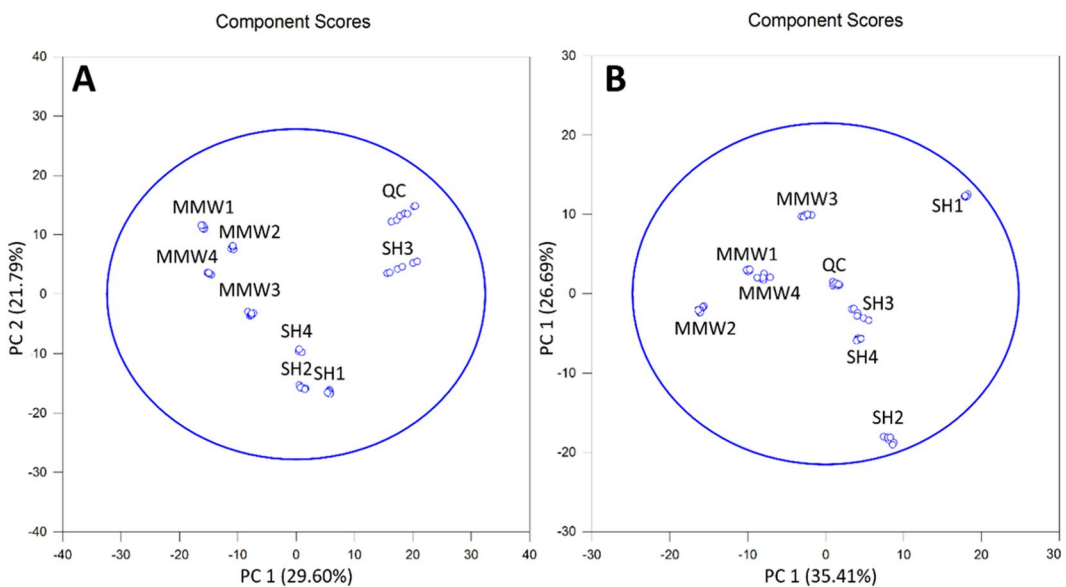


**Figure 1.** PCA plots generated from endocellular lipidomic sequences from the features displaying both a Fold-Change  $\geq 2$  and a p-value  $< 0.05$  upon R-XCMS data processing performed from UHPLC-HRMS sequences recorded in (A) Positive-Ion Mode and (B) Negative-Ion Mode. Note that  $SH_i$  (with  $i = 1$  to 4) and  $MMW_j$  (with  $j = 1$  to 4) are related to the non-exposed and exposed samples, respectively; QC represents the overall of the quality control samples.

the analytical instrumentation could also be assessed based on the clustering of the QC samples in a Principal Component Analysis (PCA) score plot of all tested sequences.

Altogether, these parameters underscore both the robustness of the LC-HRMS system operating conditions and the validity of the retrieved metabolomic data, paving the way for their statistical processing.

**Lipidomic RPLC-MS analyses.** As to intracellular fractions, the filtered data subsets were represented by 540 and 264 features, for positive and negative ionization polarities respectively. Non-exposed and exposed samples clustered separately, being discriminated along PC1 component in these two sequences (Fig. 1).

In positive and negative polarities, univariate analyses respectively identified six and four masses as the main discriminators between the two sample groups (Figs S1 and S2). Regarding positive-ion mode, tentative hits could be retrieved for two out of five species, which might correspond to ceramide derivatives and/or N-palmitoylsphingosine derivatives (Table S3). Putative matches could be proposed for two ions appearing as dysregulated in negative-ion mode, tentatively corresponding to a further ceramide derivative (Cer (d18:0/16:0)) and to a diglyceride derivative DG (36:3) (Table S4). Besides the very limited number of features appearing as dysregulated, one should note that their corresponding Fold-Change indices display modest values remaining below 5 for all features identified in the course of negative-ion mode and below 10 for those pinpointed throughout positive-ion mode analyses. The only exception was M453T283 in this latter group, for which no putative identification could be retrieved.

Filtered RPLC datasets related to extracellular fractions consisted of 289 and 126 features in positive and negative-ion modes, respectively. In both ionization modes, PCA plots accounted for roughly 60% of the total variance between the two groups. However, whatever the considered ionization mode, these plots did not lead to a clear-cut discrimination of the samples according to their exposure status (Fig. 2).

While no discriminating feature could be highlighted during the course of negative-ion mode data processing, two ions of interest could however be evidenced in positive polarity, *i.e.* M627T51 and M783T478 (Fig. S3). Putative hits could only be retrieved for this latter feature that displayed an important FC of 764, which corresponds to a phosphatidylcholine derivative with a sum composition of (36:4) (Table S5).

**Metabolomic HILIC analyses.** Endocellular data subset with features satisfying both  $FC > 2$  and ANOVA p-value  $< 0.05$  were respectively represented by 210 and 58 features in positive and negative-ion modes. Generated PCA plots roughly represented 75% of the total variance and could discriminate between non-exposed and exposed samples along PC2 component in both ion modes (Fig. 3).

Notwithstanding this discrimination, the statistical processing workflow did not lead to emphasize any relevant biomarker in the negative-ion mode data set. Positive-ion mode endometabolomics only resulted in highlighting one biomarker with a moderate FC value of 2.8 for which two putative identifications could be retrieved from HMDB database (*i.e.* either 2-aminoheptanedioic acid or N-carboxyethyl- $\gamma$ -aminobutyric acid) (Fig. S4 and Table S6).

PCA plots related to exometabolomic sequences revealed clear-cut discriminations according to millimeter wave exposure status in both polarities. Owing to the large number of features in the filtered data subset

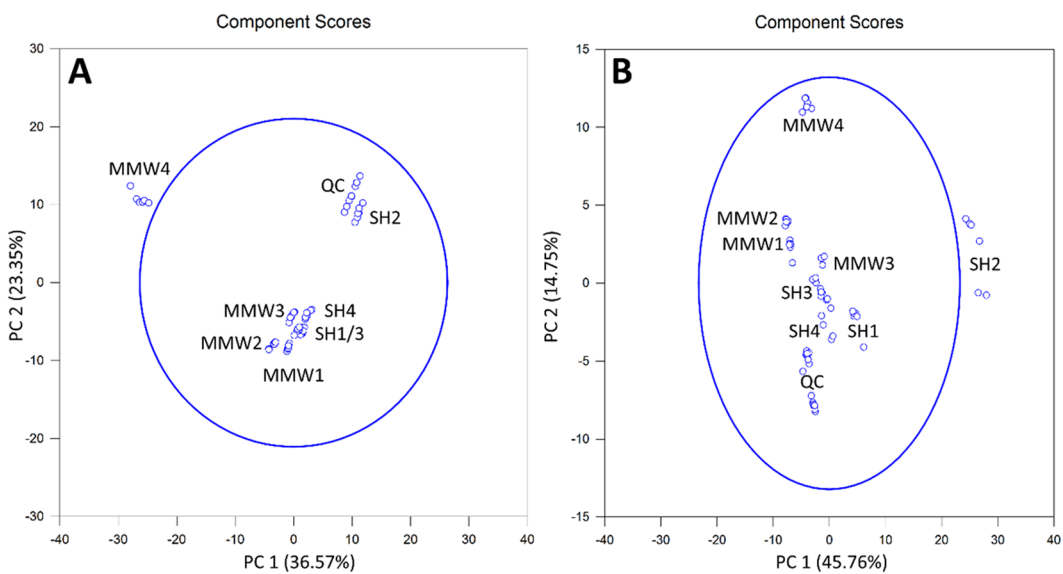


**Figure 2.** PCA plots yielded by exocellular lipidomic analyses from the ions having a Fold-Change  $\geq 2$  with a p-value  $< 0.05$  upon R-XCMS data processing performed from UHPLC-HRMS sequences recorded in (A) Positive-Ion Mode and (B) Negative-Ion Mode. Note that  $SH_i$  (with  $i = 1$  to 4) and  $MMW_j$  (with  $j = 1$  to 4) are related to the non-exposed and exposed samples, respectively; QC represents the overall of the quality control samples.

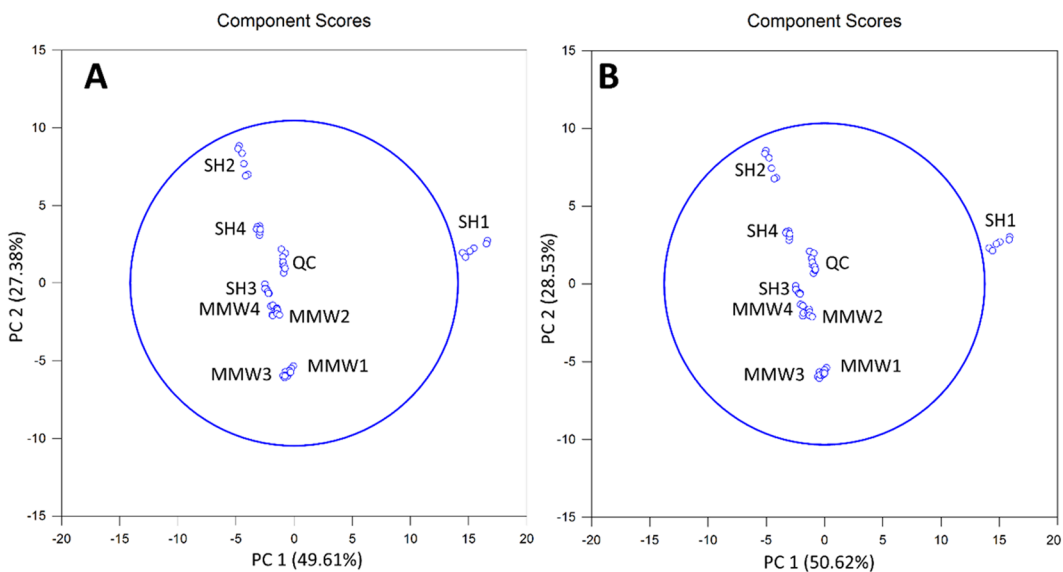


**Figure 3.** PCA plots obtained from endocellular metabolomic analyses from the features displaying both a Fold-Change  $\geq 2$  and a p-value  $< 0.05$  upon R-XCMS data processing performed from UHPLC-HRMS sequences recorded in (A) Positive-Ion Mode and (B) Negative-Ion Mode. Note that  $SH_i$  (with  $i = 1$  to 4) and  $MMW_j$  (with  $j = 1$  to 4) are related to the non-exposed and exposed samples, respectively; QC represents the overall of the quality control samples.

in positive-ion mode (662), the frames were split into two halves prior to generating the PCA plots after being ordered by increasing masses. For both these data subsets, PCA plots roughly accounted for 70% of the total variance (*ca.* 60% for PC1 and ~ 9% for PC2). In these two groups, the samples could be discriminated in a straightforward manner along PC1 component (Fig. 4A,B). Regarding negative-ion mode, the PCA plot (engulfing 506 features) accounted for 74.1% of the total variance among the two groups, where PC1 and PC2 had respective contributions of 62.7 and 8.4%. Control and exposed samples also exhibited an obvious separation along PC1 dimension (Fig. 4C).

The careful validation of both extracted ion chromatograms and box-and-whisker plot as described in the Data Processing section led applied to retainment of 111 and 99 features as dysregulated in positive and negative polarities, respectively (Figs S5 and S6). The current study was performed using a single HRMS analyser, so that

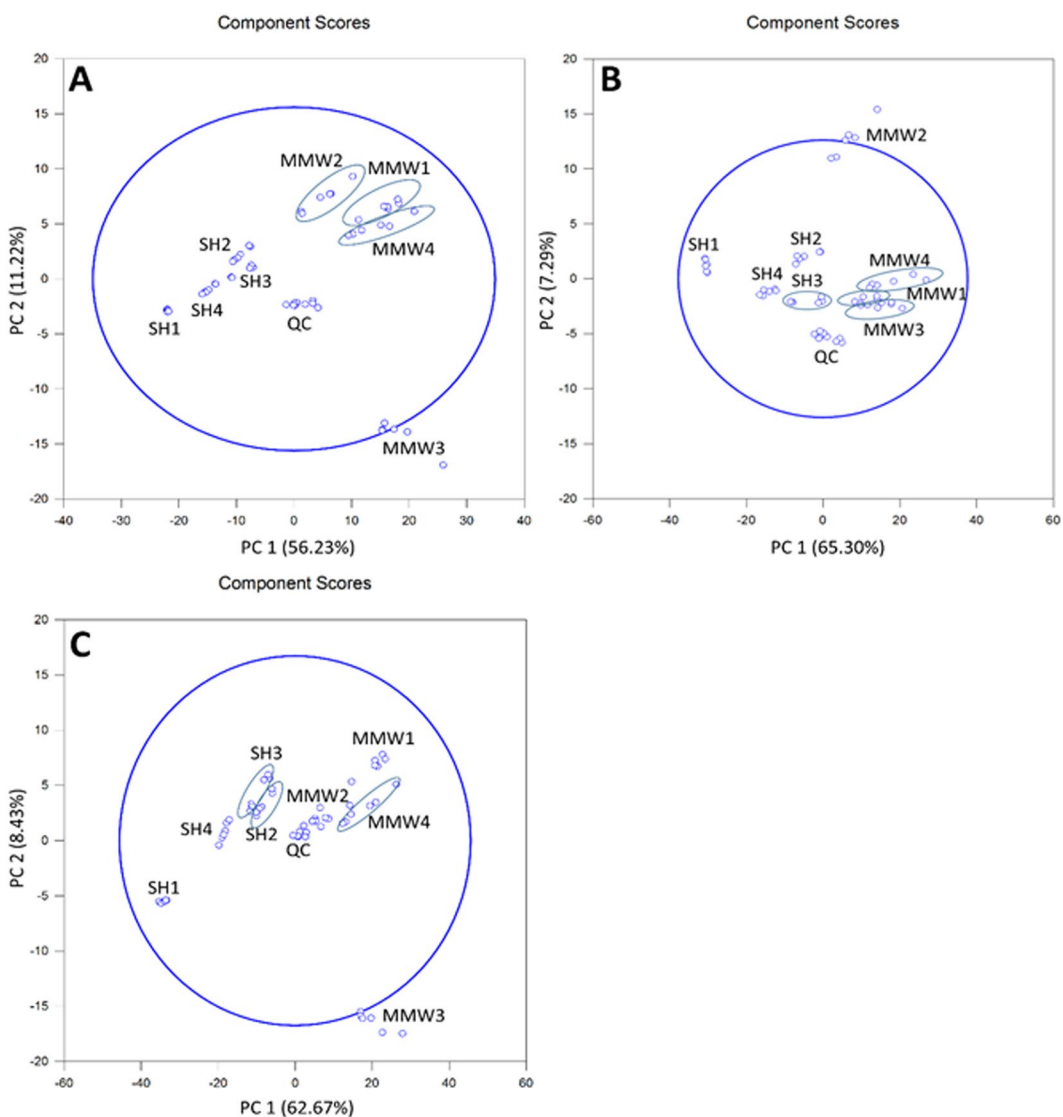


**Figure 4.** PCA plots of exocellular metabolomics sequences, selecting ions having both a FC > 2 and a p-value < 0.05 upon R-XCMS data processing performed from UHPLC-HRMS sequences recorded in (A,B) Positive-Ion Mode and (C) Negative-Ion Mode. Note that SH<sub>i</sub> (with i = 1 to 4) and MMW<sub>j</sub> (with j = 1 to 4) are related to the non-exposed and exposed samples, respectively; QC represents the overall of the quality control samples.

the identification of the dysregulated features could only rely on exact mass data, including any limitation coming along with it in terms of structural resolution. Resultantly, the structural assignments remain tentative and most often do not lead to reach unambiguous metabolites. From a practical viewpoint, handling an array of references covering the structural diversity of candidate biomarkers is not a realistic purpose in the frame of a metabolomic study pinpointing such an elevated number of features of interest. Despite this structural uncertainty, these putative identifications reveal that dysregulated features encompass an array of structurally diverse metabolites (Tables S7 and S8). Emphasizing such a large extent of dysregulations, especially in the exo-metabolomic sequences, appears as an intriguing outcome. Indeed, as upstream transcriptomics analyses did not highlight significant alterations in gene expression<sup>23</sup>, such dramatic changes would not have been expected. This led us to assume that these modifications might not be related to modifications of enzyme expression but rather stem from alterations in membrane permeability. Cell membranes are regarded as major targets for the interactions between millimeter waves and biological systems since a variety of bioeffects were reported upon exposure to these radiofrequencies<sup>25</sup>. As an example, 60 GHz exposure with an incident power density of 0.9 mW/cm<sup>2</sup> (*i.e.* in the typical range of values expected from wireless communications) was proved to induce structural modifications of artificial biomembranes. Consequently, MMW exposure was demonstrated to increase the lateral pressure of phospholipid monolayers although not strongly enough to disturb phospholipid microdomain organization in biomembranes<sup>29</sup>. Further biochemical processes could be evidenced such as the externalization of phosphatidylserine, even though the biological relevance of this event remains to be determined<sup>30</sup>. Likewise, 53-GHz

radiations and 130-GHz pulse modulated exposures were shown to alter the permeability of phospholipid vesicles<sup>31–33</sup>. MMW action on the orientation of charged and dipolar molecules in the region located between the aqueous phase and the hydrocarbon interior of the membrane has been hypothesized to represent the driving force to rearrange phospholipids bilayers, resulting in an increase of small molecules permeability across the membrane<sup>33</sup>. This new organization of the bilayer presumably displays a higher curvature which would elicit metabolites leakage. It can also be assumed that electromagnetic radiations of specific frequencies might excite components of cell membrane, depending on their electric dipoles and possibly leading to form Bose-condensed phonons<sup>34</sup>. Such assumptions are consistent with structural changes observed in cells upon MMW exposure, with different deformations being reported in bacteria<sup>35</sup>.

Likewise, it can be assumed that a similar phenomenon might trigger the leakage of intracellular metabolites into the extracellular medium shown in this manuscript. This inference is further strengthened by the huge majority of dysregulated features which are found to be upregulated in the treated group (107/111 and 98/99 in positive and negative-ion modes, respectively. It is interesting to note that under different exposure conditions, membrane permeabilization upon electric pulses of nanosecond duration were previously reported to occur in mammalian cells<sup>36,37</sup>.

## Conclusion

As far as can be ascertained, this report represents the first metabolomic investigation focusing on the effects of MMW. To get as wide an insight into cellular processes as possible, a joint metabolomic and lipidomic profiling strategy was designed and the extra and intracellular contents were discriminated. It appeared that all lipidomic sequences and intracellular metabolomic profiles were slightly affected by MMW but drastic changes in extracellular metabolomic sequences could be evidenced. During these experiments, we put great emphasis on controlling cell culture parameters (temperature, pH, incubator humidity). Much attention has been paid to temperature control, however, it cannot be ruled out that unexpected changes at subcellular scale have occurred and could be responsible for the differences found. Moreover, by making the choice to put the non-exposed control in the same place in our exposure system, we ensure that these cells are in the same growing conditions than those that are exposed. Nevertheless, it should be noted that this strategy has the disadvantage of inducing a shift of one day of culture between the control and the exposed samples. While the unusually high number of dysregulated features makes of their unambiguous structural assignment an unrealistic purpose, the current study enables drawing significant and unprecedented conclusions as to the effects of MMW exposure on cellular systems, especially when combining them with former studies carried out by our group. Accordingly, as upstream pan-transcriptomic studies in this cellular system did not lead to emphasize any significant change upon 60-GHz MMW exposure, it is reasonable to assume that the vast amount of dysregulations reported in these sequences do not stem from alterations of gene expression but rather from alterations in membrane permeability, consistently with previous reports on acellular phospholipidic systems. The tentative metabolites identified throughout the current workflow might serve as a ground to focus on subsets of metabolites through the so-called target-based metabolomics. For this purpose, multiplex LC-MS-MRM pipelines proved useful for the quantitative profiling of some of the hundreds of expected metabolites in complex biological samples with no structural/identity ambiguity. Based on the current findings, such follow-up studies could be limited to the exocellular compartment. Finally, we can conclude that our model, purely *in vitro*, haven't to be lead to a direct extrapolation of our results at the organism level. In the future, further studies will be necessary to assess MMW bioeffects on animal models and to investigate potential dysregulations induced by lower IPD values prior to the wide-scale deployment of technologies based on these specific frequencies.

## Methods

**Chemicals, reagents and materials.** LC-MS grade water, methanol (MeOH), methyl tert-butyl ether (MTBE), chloroform ( $\text{CHCl}_3$ ), acetonitrile (MeCN), 2-propanol (IPA), ammonium acetate and acetic acid were purchased from Sigma-Aldrich (St. Louis, MO, USA). The standard mixtures Calmix-positive (*i.e.* caffeine, L-methionyl-arginyl-phenylalanylalanine acetate and Ultramark 1621) and Calmix-negative (*i.e.* acetic acid, sodium dodecyl sulfate, taurocholic acid sodium salt hydrate and Ultramark 1621), were purchased from Thermo Fisher Scientific (Waltham, MA, USA).

1,2-Dipentadecanoyl-sn-glycero-3-phosphocholine (PC(15:0/15:0)), 1-pentadecanoyl-2-hydroxy-sn-glycero-3-phosphocholine (Lyso PC(15:0)), 1,2-diheptadecanoyl-sn-glycero-3-p-hosphoethanolamine (PE(17:0/17:0)) and N-heptadecanoyl-D-erythro-sphingosine (Cer(d18:1/17:0)) were obtained from Coger (Paris, France).  $^1\text{H}$ -Tryptophan-2,3,3-d<sub>3</sub> (Trypto-d<sub>3</sub>), indole-2,4,5,6,7-d<sub>5</sub>-3-acetic acid (Ind-AA-d<sub>5</sub>), 1,14-tetradecanedioic-d<sub>24</sub> acid (Tetra-A-d<sub>24</sub>) were purchased from Cluzeau Info Labo (Sainte-Foy-La-Grande, France). 1,2,3-triheptadecanoyl-glycerol (TG (17:0)), pentadecanoic acid (C15:0), tricosanoic acid (C23:0), heptadecanoic acid (C17:0), leucine-5,5,5-d<sub>3</sub> (Leu-d<sub>3</sub>), creatine-(methyl-d<sub>3</sub>) (Crea-d<sub>3</sub>) and lysine-4,4,5,5-d<sub>4</sub> (Lys-d<sub>4</sub>) were purchased from Sigma-Aldrich (St. Louis, MO, USA).

Stock standard solutions (1 mg/L) were prepared in  $\text{CHCl}_3$  (for lipidic compounds) or in MeOH and kept at  $-20^\circ\text{C}$ . The internal standard (IS) solution contains C17:0, Crea-d<sub>3</sub> and Lys-d<sub>4</sub> at 10 ng/ $\mu\text{L}$  in a MeOH/H<sub>2</sub>O mixture (4/1). Lipidomic external standard (ES) solution containing (PC (15:0/15:0), Lyso PC (15:0), PE (17:0/17:0), TG (17:0), Cer (d18:1/17:0), C15:0 and C23:0 at 0.5 ng/ $\mu\text{L}$  and metabolomic (ES) solution containing Leu-d<sub>3</sub>, Trypto-d<sub>3</sub>, Ind-AA-d<sub>5</sub> and Tetra-A-d<sub>24</sub> at 1 ng/ $\mu\text{L}$  were subsequently prepared in  $\text{CHCl}_3$  (lipidomics ES) or in MeOH (metabolomics ES).

**Cell culture.** A human keratinocyte cell line (HaCaT) was cultured as described elsewhere<sup>22</sup>. In an attempt to circumvent any senescence or drift of the cellular populations, keratinocytes were exposed at early passages (between 10 and 16). To enable proper cross-sample comparison, the quantity of cellular material was estimated

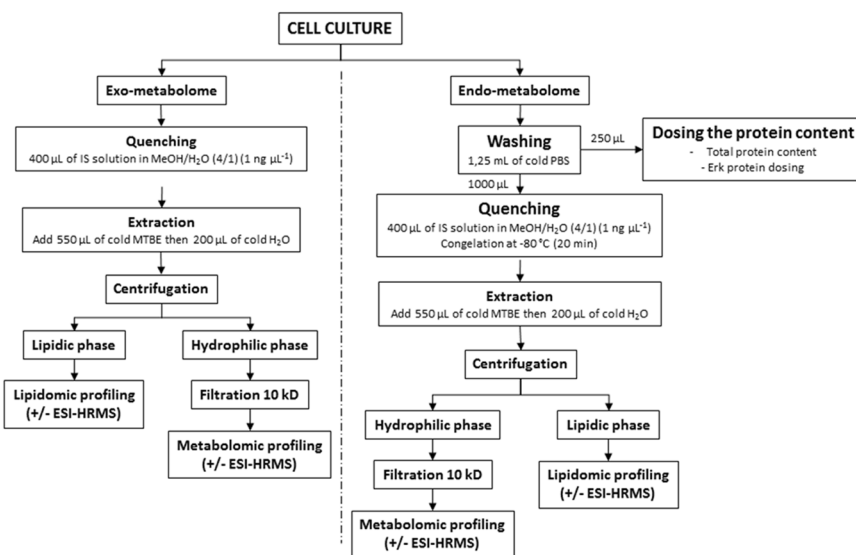


**Figure 5.** Schematic workflow of the sample preparation procedure<sup>27</sup>.

through the evaluation of total ERK protein amount (Western Blot using anti ERK1 (K-23) antibody (Santa Cruz Biotechnology, Dallas, Texas, USA))<sup>38</sup>. The exposure medium designed to keep pH buffering in the non-gassed incubator of the exposure system as described elsewhere<sup>39</sup>. Briefly, it consists in powder reconstituted DMEM medium, completed with fetal calf serum, 4-(2-hydroxyethyl)-1-piperazineethanesulfonic acid (HEPES) and antibiotics.

**Experimental setup for sample exposition.** Sample irradiation was performed as previously reported<sup>24</sup>. A thorough description of the exposure system can be found in Zhadobov *et al.*<sup>19</sup>. Briefly, a 6-well culture plate was positioned in a MEMMERT UE400 incubator to be exposed from the bottom by a standard pyramidal horn antenna. Cells were then irradiated or not by this antenna with an average incident power density (IPD) of 20 mW/cm<sup>2</sup> for 24 hours, according to the guidelines established by the International Commission on Non-Ionizing Radiation Protection (ICNIRP) for MMW with limited exposition area<sup>40</sup>. Both MMW-exposures and non-exposed samples were performed inside the same incubator, on different days. To mitigate exposure variability between sample groups, the non-exposed and MMW-Exposed cell samples were located in the same position within the same incubator<sup>39</sup>. To avoid a thermal effect associated with MMW exposure, the temperature increase was counteracted by lowering the incubator set point by the predicted increment. Consistently with literature<sup>23</sup>, MMW exposure at such IPD resulted in an elevation of 8 °C leading to set the temperature of the incubator at 28 °C in the MMW group to reach 36 °C, as in non-exposed cells. Assuming that thermal convection currents occurring in the radiofrequency-exposed groups may lead to a differential condensation of the culture medium, the consistency of the pH value was monitored in both non-exposed and exposed sample groups. An identical pH value of 7.7 could be measured from the different culture media, irrespective of their exposure status. HaCaT keratinocytes cell viability was formerly reported to be of 100% for pH values spanning across the 7.0–8.2 range<sup>41</sup>.

**Metabolomics workflow.** As MMW exposure might result in evidencing little to no biological effect, it was very important to validate the ability of the retained metabolomic workflow to emphasize the dysregulations triggered by a known interfering agent. This preliminary study, carried out using the cytotoxic drug 2-deoxyglucose, demonstrated the adequacy of the proposed workflow for metabolomics purposes<sup>27</sup>. The whole sample preparation workflow is summarized in Fig. 5.

Metabolomic analyses were carried out on 4 independent biological samples for both non-exposed and MMW-exposed groups. As to extracellular profiling, a 100-μL aliquot of the culture medium was recovered for further sample processing. Regarding intracellular metabolite assessment, the cells were washed with 1 mL of phosphate buffer solution after having discarded the remaining culture medium. The cells were subsequently detached by scraping within 1250 μL of PBS solution. A 250 μL-aliquot was recovered to evaluate the amount of total ERK, a ubiquitous protein, by western blotting. Both the endo- and exo-cellular fractions were spiked with 400 μL of Internal Standard solution dissolved in MeOH/H<sub>2</sub>O (4/1, v/v). Endocellular fractions were frozen at -80 °C for 20 minutes to facilitate cell membrane disruption. Solutions were then added with 550 μL of MTBE and vortexed three times for ten seconds (separated by one minute breaks in ice), 200 μL of cold water were then added with the same vortexing sequence being repeated. After centrifugation of the solutions (12,000 g, 4 °C, 15 min), a 300 μL-aliquot of the upper organic phase was transferred to a vial to be spiked with 40 μL of the lipidomics ES solution (0.5 ng/μL) in CHCl<sub>3</sub> prior to being dried under N<sub>2</sub> flux. The dry extract was dissolved in 200 μL of MeCN/IPA/H<sub>2</sub>O solution (65:30:5, v/v/v). Likewise, a 300 μL-aliquot of the lower aqueous phase was recovered and centrifugally filtered through a Millipore 10 kDa cutoff filter (12,000 g, 4 °C, 20 min). The solution was evaporated to dryness under N<sub>2</sub> and later resuspended in 200 μL of a MeCN/H<sub>2</sub>O (9/1, v/v) solution.

QC samples were obtained by pooling 20  $\mu\text{L}$  aliquots from the test samples to represent a bulk control sample. The samples were stored at  $-80^{\circ}\text{C}$  pending UHPLC-HRMS analysis.

**UHPLC/HRMS analyses.** Analyses were performed using an ultrahigh performance liquid chromatography (Waters Acquity), hyphenated with a Thermo QExactive mass spectrometer. Samples were injected (5  $\mu\text{L}$ ) onto either an Acquity CSH C<sub>18</sub> column (1.7  $\mu\text{m}$ , 2.1  $\times$  100 mm; Waters) for lipidomic sequences or a SeQuant ZIC-HILIC column (3.5  $\mu\text{m}$ , 2.1  $\times$  100 mm; Merck) for metabolomic HILIC analyses. The standard mobile phases for RPLC (lipidomic sequences) were A = MeCN/H<sub>2</sub>O/ammonium acetate 1 M/acetic acid (600/390/10/1, v/v/v/v) and B = IPA/MeCN/H<sub>2</sub>O/ammonium acetate 1 M/acetic acid (880/100/10/10/1, v/v/v/v/v/v). For HILIC conditions, the mobile phases were A = H<sub>2</sub>O/ammonium acetate 1 M/acetic acid (980/10/1, v/v/v) and B = MeCN/solvent A (950/50, v/v). The column oven temperature was kept constant at 35 °C for metabolomic HILIC runs and at 45 °C for lipidomic RPLC analyses. RPLC analyses were performed by gradient elution as follows: T, 0 min, 40% B; 0–2 min, 50% B linear; 2–12 min, 70% B linear; 12–17 min, 99% B linear; 17–25 min, 99% B; 25–29 min, 40% B. HILIC acquisitions were obtained using the following gradient program: T, 0–2 min, 95% B; 2–5 min, 80% B; 5–12 min, 60% B linear; 12–14 min, 40% B linear; 14–16 min, 40% B; 16–26 min, 95% B.

ESI source conditions were set as follows: sheath gas flow, 55 Arbitrary Units (AU); auxiliary gas flow, 10 AU; capillary temperature, 300 °C; spray voltage, either 3.5 kV (lipidomics) or 3.0 kV (metabolomics); S-lens radiofrequency, 50 AU. Mass spectra were either acquired over the *m/z* range 150–1500 (lipidomics) or 65–975 (metabolomics) at a resolving power of 35000 Full Width Half Maximum (FWHM) measured at *m/z* 200. The Automatic Gain Control (AGC target) was set at high dynamic range ( $5 \times 10^5$ ) with a maximum injection time of 100 ms. External calibrations of the MS instrument were performed using the Calmix-positive and Calmix-negative standard solution for the positive and the negative ionization modes, respectively. Exact mass measurements did not take into account the mass of the electron.

The analytical run was initiated by a number of injections of QC samples to ensure that LC and MS systems had time to equilibrate and perform satisfactorily. Irrespective of their exposed or non-exposed sample status, the study samples were randomized to limit the effect of time trends and thus minimize bias introduced by non-biological parameters (e.g. instrumental drifts). Each sample was analyzed six times.

**Statistical processing.** The statistical processing of the metabolomic data considered all exposed and unexposed samples independently of one another. LC/MS data were further processed by R package XCMS (version 3.2). The preprocessing results generated a data matrix as a feature list table comprising their integrated intensities (reconstructed ion chromatogram peak areas), along with the observed fold-changes and associated p-values<sup>42</sup>. Applied peak picking parameters were prefilter = c(5,25), snthresh = 6, mzdiff = 0.01 and ppm = 15. Initial alignment (bw = 20, minfrac = 0.66, minsamp = 4, mzwid = 0.008) and retention time correction (standard loess, plottype = c(deviation) were then applied. Further alignment steps were performed using the same processing parameters with decreasing bw values (lowered to bw = 9 for the second round and to 5 for the final stage). Subsequently, R-package CAMERA was used for peak annotation after XCMS data processing<sup>43</sup>. Consistently with reported guidelines, features found in less than 20% of the analyzed samples were removed according to the so-called 80% rule<sup>44</sup>.

As to univariate analyses, the coefficient of variation (CV) within QC samples was calculated by dividing the standard deviation by the mean intensity of each feature, leading to a histogram of the resulting CV distribution. Subsequently, computation of the Fold-Change (FC, ratio of abundance between non-exposed and exposed samples) along with the corresponding p-value (statistical significance from a Student t-test) streamlined the selection of metabolites of interest. Features selection was based on the following criteria: CV QC < 30%, FC > 2 and ANOVA p-value < 0.05. Extracted Ion Chromatograms (EICs) were individually monitored to exclude potential artifacts from the ion list. Later on, Box and Whiskers Plot related to all metabolites of potential interest were also individually checked to retain the features for which no overlap existed between values obtained from non-exposed and exposed samples. Such features were tentatively identified against databases as described later on. The top and bottom of each box represent the 25<sup>th</sup> and 75<sup>th</sup> percentiles, the center line indicates the median and the extent of the whiskers depicts the 5<sup>th</sup> and 95<sup>th</sup> percentiles. Regarding multivariate analyses, Principal Component Analyses (PCA) were performed to get a general overview of the interrelationship between study samples as well as QC. Statistical graphs were prepared using SigmaPlot 13.0® (Systat Software, Inc., USA). Filtered data sets related to each sequence (only retaining features displaying FC > 2 and p-value < 0.05) were then analyzed by PCA to explore samples' relationship and grouping. For this purpose, PCA retrieves a small number of principal components that summarize the measured data to visualize trends and emphasize possible outliers.

**Metabolite identification.** [M + H]<sup>+</sup>, [M-H<sub>2</sub>O + H]<sup>+</sup>, [M + Na]<sup>+</sup> and [M-H<sub>2</sub>O + Na]<sup>+</sup> were selected as possible adducts for positive polarity. Regarding negative-ion mode, [M-H]<sup>-</sup>, [M-H<sub>2</sub>O-H]<sup>-</sup> and [M-H<sub>2</sub>O + HCOOH-H]<sup>-</sup> were considered. Putative identifications were carried out against the freely available database Human Metabolome Data Base (HMDB). Whenever possible, efforts were made to narrow down identification possibilities among isobaric compounds according to elution order, matrix of occurrence.

## Data Availability

The datasets generated and analysed during the current study are available from the corresponding author on reasonable request. The accession number for the metabolomics data reported in this paper are Massive MSV000083829.

## References

- Alavi, S. E. *et al.* Towards 5G: A photonic based millimeter wave signal generation for applying in 5G access fronthaul. *Sci. Rep.* **6**, 19891 (2016).
- Pakhomov, A. G., Akyel, Y., Pakhomova, O. N., Stuck, B. E. & Murphy, M. R. Current state and implications of research on biological effects of millimeter waves: a review of the literature. *Bioelectromagnetics* **19**, 393–413 (1998).
- Zhadobov, M., Chahat, N., Sauleau, R., Le Quement, C. & Le Drean, Y. Millimeter-wave interactions with the human body: State of knowledge and recent advances. *Int. J. Microw. Wirel. Technol.* **3**, 237–247 (2011).
- Radzievsky, A. A. *et al.* Electromagnetic millimeter wave induced hypoalgesia: frequency dependence and involvement of endogenous opioids. *Bioelectromagn. J. Bioelectromagn. Soc. Soc. Phys. Regul. Biol. Med. Eur. Bioelectromagn. Assoc.* **29**, 284–295 (2008).
- Ziskin, M. C. Millimeter waves: Acoustic and electromagnetic. *Bioelectromagnetics* **34**, 3–14 (2013).
- Alekseev, S. I., Gordienko, O. V., Radzievsky, A. A. & Ziskin, M. C. Millimeter wave effects on electrical responses of the sural nerve *in vivo*. *Bioelectromagn. J. Bioelectromagn. Soc. Soc. Phys. Regul. Biol. Med. Eur. Bioelectromagn. Assoc.* **31**, 180–190 (2010).
- Wu, T., Rappaport, T. S. & Collins, C. M. The human body and millimeter-wave wireless communication systems: Interactions and implications. *In Communications (ICC), 2015 IEEE International Conference on* 2423–2429 (IEEE, 2015).
- Grundler, W., Keilmann, F. & Fröhlich, H. Resonant growth rate response of yeast cells irradiated by weak microwaves. *Phys. Lett. A* **62**, 463–466 (1977).
- Grundler, W., Kaiser, F., Keilmann, F. & Wallczek, J. Mechanisms of electromagnetic interaction with cellular systems. *Naturwissenschaften* **79**, 551–559 (1992).
- Grundler, W. & Kaiser, F. Experimental evidence for coherent excitations correlated with cell growth. *Nanobiology* **1**, 163–176 (1992).
- Kataev, A. A., Alexandrov, A. A., Tikhonova, L. L. & Berestovsky, G. N. Frequency-dependent effects of the electromagnetic millimeter waves on the ion currents in the cell membrane of *Nitellopsis*: Nonthermal action. *Biofizika* **38**, 446–462 (1993).
- Belyaev, I. Y., Alipov, Y. D., Shcheglov, V. S., Polunin, V. A. & Aizenberg, O. A. Cooperative response of *Escherichia coli* cells to the resonance effect of millimeter waves at super low intensity. *Electro-Magnetobiology* **13**, 53–66 (1994).
- Gandhi, O. P., Hagmann, M. J., Hill, D. W., Partlow, L. M. & Bush, L. Millimeter wave absorption spectra of biological samples. *Bioelectromagn. J. Bioelectromagn. Soc. Soc. Phys. Regul. Biol. Med. Eur. Bioelectromagn. Assoc.* **1**, 285–298 (1980).
- Bush, L. G. *et al.* Effects of millimeter-wave radiation on monolayer cell cultures. III. A search for frequency-specific athermal biological effects on protein synthesis. *Bioelectromagn. J. Bioelectromagn. Soc. Soc. Phys. Regul. Biol. Med. Eur. Bioelectromagn. Assoc.* **2**, 151–159 (1981).
- Kazarinov, K. D., Sharov, V. S., Putvinskii, A. & Betskii, O. The effect of continuous millimeter low-intensity radiation on the Na<sup>+</sup> ion transport in the frog skin. *Biofizika* **29**, 480–482 (1984).
- Furia, L., Hill, D. W. & Gandhi, O. P. Effect of millimeter-wave irradiation on growth of *Saccharomyces cerevisiae*. *IEEE Trans. Biomed. Eng.* 993–999 (1986).
- Khramov, R. N., Sosunov, E. A., Koltun, S. V., Ilyasova, E. N. & Lednev, V. V. Millimeter-wave effects on electric activity of crayfish stretch receptors. *Bioelectromagnetics* **12**, 203–214 (1991).
- Adair, R. K. Biophysical limits on athermal effects of RF and microwave radiation. *Bioelectromagnetics* **24**, 39–48 (2003).
- Zhadobov, M. *et al.* Low-power millimeter wave radiations do not alter stress-sensitive gene expression of chaperone proteins. *Bioelectromagnetics* **28**, 188–196 (2007).
- Nicolaz, C. N. *et al.* Study of narrow band millimeter-wave potential interactions with endoplasmic reticulum stress sensor genes. *Bioelectromagnetics* **30**, 365–373 (2009).
- Nicolaz, C. N. *et al.* Absence of direct effect of low-power millimeter-wave radiation at 60.4 GHz on endoplasmic reticulum stress. *Cell Biol. Toxicol.* **25**, 471–478 (2009).
- Le Quément, C. *et al.* Impact of 60-GHz millimeter waves and corresponding heat effect on endoplasmic reticulum stress sensor gene expression. *Bioelectromagnetics* **35**, 444–451 (2014).
- Habauzit, D. *et al.* Transcriptome analysis reveals the contribution of thermal and the specific effects in cellular response to millimeter wave exposure. *PLoS One* **9**, e109435 (2014).
- Soubere Mahamoud, Y. *et al.* Additive effects of millimeter waves and 2-deoxyglucose co-exposure on the human keratinocyte transcriptome. *PLoS One* **11**, e0160810 (2016).
- Ramundo-Orlando, A. Effects of millimeter waves radiation on cell membrane-A brief review. *J. Infrared Millim. Terahertz Waves* **31**, 1400–1411 (2010).
- Zhadobov, M. *et al.* Near-field dosimetry for *in vitro* exposure of human cells at 60 GHz. *Bioelectromagnetics* **33**, 55–64 (2012).
- Le Pogam, P. *et al.* Untargeted Metabolomics Reveal Lipid Alterations upon 2-Deoxyglucose Treatment in Human HaCaT Keratinocytes. *J. Proteome Res.* **17**, 1146–1157 (2018).
- Gika, H. G., Theodoridis, G. A., Plumb, R. S. & Wilson, I. D. Current practice of liquid chromatography-mass spectrometry in metabolomics and metabolomics. *J. Pharm. Biomed. Anal.* **87**, 12–25 (2014).
- Zhadobov, M. *et al.* Interactions between 60-GHz millimeter waves and artificial biological membranes: dependence on radiation parameters. *IEEE Trans. Microw. Theory Tech.* **54**, 2534–2542 (2006).
- Szabo, I., Kappelmayer, J., Alekseev, S. I. & Ziskin, M. C. Millimeter wave induced reversible externalization of phosphatidylycerine molecules in cells exposed *in vitro*. *Bioelectromagnetics* **27**, 233–244 (2006).
- Ramundo-Orlando, A. *et al.* Permeability changes induced by 130 GHz pulsed radiation on cationic liposomes loaded with carbonic anhydrase. *Bioelectromagn. J. Bioelectromagn. Soc. Soc. Phys. Regul. Biol. Med. Eur. Bioelectromagn. Assoc.* **28**, 587–598 (2007).
- Ramundo-Orlando, A. *et al.* The response of giant phospholipid vesicles to millimeter waves radiation. *Biochim. Biophys. Acta BBA-Biomembr.* **1788**, 1497–1507 (2009).
- Di Donato, L., Cataldo, M., Stano, P., Massa, R. & Ramundo-Orlando, A. Permeability changes of cationic liposomes loaded with carbonic anhydrase induced by millimeter waves radiation. *Radiat. Res.* **178**, 437–446 (2012).
- Anton, E. *et al.* Links between extremely high frequency electromagnetic waves and their biological manifestations. *Arch. Biol. Sci.* **67**, 895–897 (2015).
- Torgomyan, H., Hovnanyan, K. & Trchounian, A. *Escherichia coli* growth changes by the mediated effects after low-intensity electromagnetic irradiation of extremely high frequencies. *Cell Biochem. Biophys.* **65**, 445–454 (2013).
- Teissie, J., Golzio, M. & Rols, M. P. Mechanisms of cell membrane electroporation: a minireview of our present (lack of?) knowledge. *Biochim. Biophys. Acta BBA-Gen. Subj.* **1724**, 270–280 (2005).
- Pakhomov, A. G. *et al.* Membrane permeabilization and cell damage by ultrashort electric field shocks. *Arch. Biochem. Biophys.* **465**, 109–118 (2007).
- Kerdivel, G. *et al.* Activation of the MKL1/actin signaling pathway induces hormonal escape in estrogen-responsive breast cancer cell lines. *Mol. Cell. Endocrinol.* **390**, 34–44 (2014).
- Haas, A. J. *et al.* Impact of 60-GHz millimeter waves on stress and pain-related protein expression in differentiating neuron-like cells. *Bioelectromagnetics* **37**, 444–454 (2016).
- Ahlborn, A. *et al.* Guidelines for limiting exposure to time-varying electric, magnetic, and electromagnetic fields (up to 300 GHz). *Health Phys.* **74**, 494–521 (1998).

41. Dias, K., de, C., Barbugli, P. A. & Vergani, C. E. Influence of different buffers (HEPES/MOPS) on keratinocyte cell viability and microbial growth. *J. Microbiol. Methods* **125**, 40–42 (2016).
42. Smith, C. A., Want, E. J., O'Maille, G., Abagyan, R. & Siuzdak, G. XCMS: processing mass spectrometry data for metabolite profiling using nonlinear peak alignment, matching, and identification. *Anal. Chem.* **78**, 779–787 (2006).
43. Kuhl, C., Tautenhahn, R., Bottcher, C., Larson, T. R. & Neumann, S. CAMERA: an integrated strategy for compound spectra extraction and annotation of liquid chromatography/mass spectrometry data sets. *Anal. Chem.* **84**, 283–289 (2011).
44. Bijlsma, S. *et al.* Large-scale human metabolomics studies: a strategy for data (pre-) processing and validation. *Anal. Chem.* **78**, 567–574 (2006).

## Acknowledgements

The authors are indebted to the French Agency for Food, Environmental and Occupational Health and Society (ANSES) for having funded this study through the project BEMAM (BioElectroMagnétisme et Analyse Métabolomique – n° EST-2014/2 RF/012). Metabolomic analyses used the instrumental facilities of LABERCA (Nantes).

## Author Contributions

P. Le Pogam performed experiments, analyzed data and mainly wrote the manuscript. Y. Le Page and D. Habauzit performed experiments and contributed to the design of the biology-related aspects of the manuscript. M. Doué contributed to the technical validation of the metabolomic pipeline reported herein. M. Zhadobov and R. Sauleau supervised the radiofrequency exposure related aspects of the manuscript. Y. Le Dréan mainly designed the biology-related research of the manuscript. D. Rondeau designed experiments, supervised the analytical chemistry-related content of this investigation, and contributed to the analysis of the data and to the writing of the manuscript. All authors reviewed and approved the final version of the manuscript.

## Additional Information

**Supplementary information** accompanies this paper at <https://doi.org/10.1038/s41598-019-45662-6>.

**Competing Interests:** The authors declare no competing interests.

**Publisher's note:** Springer Nature remains neutral with regard to jurisdictional claims in published maps and institutional affiliations.



**Open Access** This article is licensed under a Creative Commons Attribution 4.0 International License, which permits use, sharing, adaptation, distribution and reproduction in any medium or format, as long as you give appropriate credit to the original author(s) and the source, provide a link to the Creative Commons license, and indicate if changes were made. The images or other third party material in this article are included in the article's Creative Commons license, unless indicated otherwise in a credit line to the material. If material is not included in the article's Creative Commons license and your intended use is not permitted by statutory regulation or exceeds the permitted use, you will need to obtain permission directly from the copyright holder. To view a copy of this license, visit <http://creativecommons.org/licenses/by/4.0/>.

© The Author(s) 2019